Orbit Determination of Highly Elliptical Earth Orbiters Using VLBI and ΔVLBI Measurements

R. B. Frauenholz
J. Ellis
Navigations Systems Section

This paper shows the feasibility of using Very Long Baseline Interferometric data acquired by the Deep Space Network to navigate highly elliptical Earth orbiting satellites. The mission orbit of the Ion Release Module of the Active Magnetospheric Particle Tracer Explorers is used as a reference for developing strategies and provides the first opportunity for a possible flight demonstration with a spacecraft in a highly elliptical orbit.

The navigation accuracy improvements achievable with VLBI and ΔVLBI data types are determined for comparison with the doppler capability. Preferred VLBI data acquisition strategies are developed to achieve optimum navigation performance and to minimize antenna support requirements. The sensitivity of the VLBI navigation accuracy to the baseline orientation relative to the orbit plane is examined, as are the effects of major error sources such as gravitational harmonics and atmospheric drag.

The results showed that strategies using wideband ΔVLBI measurements taken near periapse performed best, determining the apoapse position to an order of magnitude better than conventional doppler. A similar approach using narrowband ΔVLBI near periapse achieves results comparable to the doppler capability. Overall, VLBI measurements perform as well or better than strategies using conventional doppler, while substantially reducing the required antenna support.

I. Introduction

For many years both Earth-orbiting and interplanetary spacecraft have been successfully navigated using conventional radio metric doppler and range measurements acquired by a worldwide network of ground stations. These techniques have served well but have often required either numerous or long data acquisition passes to achieve the desired navigation accuracies. As the number of missions to be supported increases and navigation accuracies become more demanding, resulting increases in antenna committments often lead to overloading. The recent development and application of Very Long Baseline Interferometry (VLBI) technology have served not only to improve the achievable navigation accuracies for

deep space missions such as Voyager, but also to reduce the antenna support needed for these missions.

Future interplanetary navigation is expected to rely on VLBI for the determination of the geocentric angular position and velocity of deep space probes (Ref. 1). This technique uses two widely separated tracking stations to simultaneously receive a signal broadcast by a beacon onboard the spacecraft. Cross-correlation of the received signals provides a precise measure of the differential time delay for wide bandwidth signals, and the rate of change of time delay for narrow bandwidth signals. By alternately tracking the probe and a nearby extra galactic radio source (EGRS, or quasar) of known location, a doubly-differenced one-way measurement (ΔVLBI) is constructed which is insensitive to major error sources common to each downlink. Differencing the two signals cancels common ground and spacecraft error sources and reduces the effects of transmission media, timing, polar motion, and station location uncertainties. The degree of error reduction depends on the spacecraft-quasar angular separation. In addition to eliminating the need for an uplink, the VLBI technique significantly reduces the antenna support requirements, with a typical measurement requiring from 5 to 10 minutes of acquisition time.

Two basic types of ΔVLBI measurements have been used for deep space navigation. For a spacecraft with a wideband transponder, a differential one-way range (ΔDOR) is acquired with a typical 1σ random measurement error of 15 cm. If only a narrow band spacecraft signal is available then the ΔVLBI technique provides a measure of the instantaneous rate of change of the delay with a typical 1σ accuracy of 0.1 mm/s. Observations from two nearly orthogonal baselines are required to simultaneously resolve the geocentric right ascension and declination.

A restricted bandwidth form of ΔDOR is currently being used for Voyager navigation. With a bandwidth of 14 Mhz, accuracies of 70 nanoradians have been achieved (Ref. 2). Galileo will be the first deep space mission to carry a wideband transponder specifically for ΔDOR acquisition. With the 38 Mhz bandwidth, accuracies of 50 nanoradians are expected (J. B. Thomas, "An Error Analysis for Galileo Angular Position Measurements with the Block I ΔDOR System," JPL Internal Memorandum, EM 335-26, Nov., 1981). The narrowband form has proven to be primarily useful for navigation of planetary orbiters. Covariance studies have shown that for a low altitude circular orbiter such as the Venus Orbiting Imaging Radar mission, narrowband data are necessary to determine the orbit plane orientation (Ref. 3).

There are future plans to demonstrate the use of ΔDOR for geosynchronous orbit determination using data acquired from the Air Force DSCC II satellite. Covariance studies have shown a potential accuracy of 5–10 meters can be achieved for this application (Ref. 4).

For deep space applications, the heliocentric angular position and velocity of the probe are relatively constant over a single overlap period. Because of the large distance between the probe and the stations, we may assume that the topocentric and geocentric directions to the probe are equal; hence a DOR observation will determine the angle between the station baseline and the direction to the probe. For a highly elliptical Earth orbiter, DOR observations that are not near periapse will provide similar angular information. Since the angular change for an Earth orbiter may be considerable over a single overlap period, frequent DOR measurements across the overlap will also provide precise angular rate information.

In this paper we wish to determine the navigation accuracies achievable for a highly elliptical Earth orbiter using ΔDOR, DOR, and NBΔVLBI measurements for direct comparison with the capabilities of conventional two-way doppler and range. We will also define a convenient means of observing the information content of VLBI measurements in terms of orbit geometry. First we will describe the DSN station viewing geometries of the reference orbit for the acquisition of both conventional and VLBI measurements.

II. The Reference Orbit and DSN Viewing Geometries

A. Reference Orbit

Our reference orbit, that of the AMPTE/IRM spacecraft, is 550 km × 17.7 R_e altitude with an inclination of 28.7 deg. The time and altitude history of this orbit, shown in Fig. 1, indicates that the spacecraft spends all but one hour of each orbital period beyond 1 R_e. With a period of 43.8 hrs, a series of unique viewperiods by DSN ground stations are provided during 11-day intervals while the spacecraft completes 6 orbital periods.

B. DSN Viewperiods

The viewperiods of the DSN complexes at Goldstone, Madrid, and Canberra are related to orbit position in Fig. 2. We see that nearly all regions about the orbit are covered by the three complexes, with several tracking passes also including periapse. Similar, but not identical, viewperiod sets are repeated during subsequent 11-day intervals. This viewing geometry provides generous opportunities to acquire conventional radio metric doppler and range measurements at almost any position in the orbit.

To acquire measurements for generating the VLBI and ΔVLBI data types, simultaneous viewing by two of the DSN

complexes is needed. The three DSN complexes form three different baselines to acquire these measurements. While we will not concern ourselves with other orbit geometries in this paper, it is important to note that the number and length of overlaps increase with orbital period and apoapse height, and that the orbital inclination dictates which stations provide the overlaps. Because of the 28.7-deg inclination of our reference orbit, we found overlaps only from the Goldstone-Canberra and the Goldstone-Madrid baselines. There are two possible viewperiod overlaps from each of these baselines during each orbital period. A composite of the visible overlaps during a 7-orbit sequence is shown for each baseline in Fig. 3. There are a total of 9 overlaps available for the Goldstone-Canberra baseline during the initial 11-day cycle; there are 8 for Goldstone-Madrid. These overlaps are sequentially numbered and are shown to walk through the orbit, providing a different geometric view of the orbit with each overlap. An odd-even numbering scheme has been selected to indicate the expected occurrence of two overlaps during each orbital period. When a second overlap is not visible it is identified, for example, as overlap number 13. The 12th overlap for each baseline occurs during the 7th orbit and is included to illustrate the repetition of the viewing geometry following the fundamental 6-orbit cycle. Table 1 lists the individual orbit numbers identified in Fig. 3, and defines the duration and total true anomaly change of each visible overlap

III. Navigation System Error Model

Our reference orbit spends approximately 90% of the 43.8-hr period beyond 5 R_e, as shown in Fig. 1. Such an orbit increases the effects of solar and lunar gravitational perturbations, causing the periapse altitudes over an annual cycle to be as low as 290 km (Ref. 5). This results in measurable atmospheric drag and increases the orbit sensitivity to uncertainties in the Earth's geopotential field and gravitational constant (GM).

The error model used in this navigation study includes the effects of uncertainties in the Earth's geopotential field and GM, the lunar GM and ephemeris, solar pressure and flux, atmospheric drag coefficient, and tropospheric refraction. In addition, the effects of station location and timing uncertainties on the accuracy of the orbit are also modelled. The 1σ uncertainties in each error source are presented in Table 2. These error sources will be treated as considered parameters in a batch filter process in which we will usually estimate only the spacecraft state prior to the data arc.

In this study uncertainties in the Earth's geopotential field are represented by a lumped parameter model, defined by scaling the difference between two independent geopotential models. In our study we use 75% of the difference between APL (Applied Physics Laboratory) and SAO (Smithsonian Astrophysical Observatory) 8 X 8 models to represent the uncertainty in the geopotential field. It will later be shown that this error source dominates the total achievable navigation accuracy when using VLBI for our Earth orbiter application, and that the achievable navigation accuracy may be improved by using a more accurate geopotential model.

IV. Navigation Capability Using Doppler and Range

The navigation capability using conventional two-way doppler and range is established to provide a reference against which the performance of candidate strategies using VLBI and ΔVLBI can be compared. This reference represents an operationally realistic navigation strategy capable of satisfying orbit accuracy for both science and DSN antenna acquisition requirements for an IRM-like orbit. We have conservatively restricted our data acquisition strategies to viewperiods ±90 deg of true anomaly away from periapse (±28 min) to avoid the possible presence of high antenna-relative angular rates.

To develop our reference strategy we first examined the use of doppler alone, initially for a single station at each DSN complex, then for each of the three possible two-complex pairs, and finally for a station from each of the three complexes. These strategies were analyzed using the navigation system error model presented in Table 2. We have considered each error source while estimating only the spacecraft state. In each case the definitive orbit accuracy was based on a single 30-min pass per day for each station for 10 consecutive days. These passes were taken from the center of each available viewperiod (see Fig. 2). Orbit errors were then propagated for an additional 10 days. The largest definitive position uncertainties were found to occur near apoapse. The 3σ RSS apoapse position accuracies achievable by different station combinations are compared to a typical 3σ DSN antenna acquisition requirement in Fig. 4. The best single-station performance is obtained by Goldstone, while the best two-station strategy is provided by the Goldstone-Canberra combination. When data from Madrid are added to those data from the Goldstone-Canberra pair, very little improvement in orbit accuracy is realized. Adding a single range point to each doppler pass also results in only modest improvements. Therefore, we have chosen to adopt the Goldstone-Canberra strategy using doppler alone as our reference capability for conventional radio metric data.

In Fig. 5 we have decomposed the total 1σ RSS position uncertainties for the doppler strategy into the individual contributions due to data noise and considered parameters. Data noise errors are decomposed into radial, cross-track, and along-track components. In the definitive phase, data noise

dominates the total position uncertainty, with maximum RSS totals occurring near apoapse. The radial component was determined most accurately, as expected for a doppler strategy, while the relatively large magnitude of the cross-track component indicates the difficulty of using doppler to determine orbit plane orientation. In the predictive phase, on the other hand, total position uncertainty was dominated by considered parameters. By this time accumulating velocity errors due to gravitational harmonics resulted in orbital period errors which shifted associated position errors to the periapse region.

A breakdown of the total position error into the contributions of data noise and considered parameters is presented in Fig. 6 for both the apoapse and periapse regions of the orbit. Near apoapse both definitive and predictive phases perform similarly, with uncertainties dominated by data noise. The smaller effects of the considered parameters are primarily due to the Earth's geopotential field and gravitational constant, and to a lesser extent to atmospheric drag. Near periapse both the definitive and predictive uncertainties are dominated by errors in the geopotential field. Accuracy improvement near apoapse is best achieved by increasing the amount of data to overcome the effects of the data noise, rather than by estimating one or more of the considered parameters. To improve the accuracy near periapse would require an improved estimate of the geopotential field. Because we are representing this error source as a lumped parameter, we could not isolate the effects of individual harmonics in our estimation process.

V. Navigation Strategies Using VLBI Data

A. VLBI Data Content

In this section our objective is to qualitatively anticipate the characteristics of VLBI data value for a highly elliptical Earth orbiter based on our experience with deep space applications. The covariance analysis used to estimate the navigation performance will examine the sensitivity of VLBI strategies to orbit geometry, data sampling rate, and baseline selection.

Geocentric angular position and velocity are relatively constant for deep space probes across typical VLBI data acquisition viewperiods. As a result, the use of weekly ΔDOR observations is adequate. Velocity and acceleration estimates are obtained by sampling over intervals up to several weeks. The motion of the probe relative to the central body is inferred from a combination of dynamic modelling and angular accelerations. By comparison, the time scale for our highly elliptical orbiter application is considerably compressed. Geocentric angular changes may be very large over a single ΔDOR viewing opportunity. Consequently, data strategies using frequent sampling over a single pass may be quite typical.

The VLBI measurement provides an instantaneous measure of the angle between the baseline and the probe. If the baseline lies entirely in the orbit plane, successive VLBI measurements would provide in-plane angular position and angular rates relative to this baseline. A baseline orthogonal to the plane would yield information about the orbit plane orientation. The time history of the angle between the baseline and the projection of the baseline in the orbit plane, which is displayed in Fig. 7, shows that the Goldstone-Canberra baseline inclination angle varies from 62 to 72 deg, and from 12 to 30 deg for Goldstone-Madrid. Based on these trends, we may expect that data from both baselines will be required to resolve both the position and velocity.

In addition to the average trend of the inclination histories, we are also interested in the variation within each overlap. When the variation is greatest we can expect to observe the greatest change in baseline-relative spacecraft motion since all overlaps will have Earth-rotation effects in common. In Fig. 7 the #8 overlap for the Goldstone-Madrid baseline has an inclination trend which is dramatically different from those of all the other overlaps shown for either baseline. Figure 3 illustrates that this overlap occurs near periapse, and that there are only two such overlaps available during the 11-day cycle, one for each baseline. We will later demonstrate that there is considerably more information content in these two overlaps than in all of the other available overlaps combined.

B. Navigation Strategies Using ΔDOR

Initially the navigation capabilities using ΔDOR strategies are developed and compared with DOR strategies, and then both are compared to our reference doppler capabilities. The use of ΔDOR requires the availability of a nearby quasar, as the improved accuracy of this measurement results from the elimination of station clock synchronization errors and the reduction of sensitivity to media effects by differencing spacecraft and quasar VLBI observables. We have assumed quasar availability and have used the ΔDOR noise and bias values in Table 2 for our studies.

To develop our ΔDOR strategies we separately examined the performance for each baseline using all overlaps visible during the 11-day cycle (Fig. 3). To reflect changes in information content across each overlap in our analysis, a single measurement near the beginning, the middle, and the end of each overlap was selected. We first examined the capability using only the center measurement, then both end points, and finally all three points. From this process it was determined that the Goldstone-Canberra baseline performed somewhat better than Goldstone-Madrid. Figure 8(b) compares the capability of the 1-, 2-, and 3-point strategies for the Goldstone-Canberra baseline, illustrating the 1σ RSS position uncertainty for a 10-day definitive period and a predictive interval of an additional

10 days. The definitive accuracy of the 2-point strategy is an order-of-magnitude better than the single-point case and performed essentially the same as the 3-point strategy. We observe better performance from the multiple-point strategies because these measurements are acquired at different true anomalies, providing in-plane angular position information across the overlap that is not possible using the single measurement. All three ΔDOR strategies demonstrate similar predictive uncertainties due to the dominating influence of gravitational harmonics. One can also see that the capability of the single-point strategy compares favorably with the doppler capability provided for reference in Fig. 8(a). At once we see a means of matching the doppler results, but with significantly fewer measurments. With these results we adopted the 2-point strategy as a ΔDOR reference for comparison with other possibilities.

Our next objective was to understand the sensitivity of the measurements from each overlap as a function of orbit geometry. We earlier alleged, using data in Fig. 7 and Table 2, that large changes in the true anomaly during an overlap reflected large changes in baseline-relative spacecraft dynamics, and that we might expect to benefit from such geometry. In fact, we have already witnessed this effect in arriving at our 2-point reference strategy. Not surprisingly, Table 2 identifies the largest changes in true anomaly as occuring near periapse. To gain a measure of the data strength of the single periapse overlap contained in our Goldstone-Canberra baseline, we removed it from our data set. The capabilities of the 2-point strategy with and without the data from the single periapse overlap are compared in Fig. 8(c). Here, the definitive orbit accuracy degrades an order-of-magnitude when the periapse data is omitted, and tends to perform similar to our doppler strategy. However, both strategies yield similar maximum predictive accuracies due to the dominant effects of uncertainties in the Earth's geopotential field.

With the influence of the periapse data established, we next evaluated the performance using only the periapse data. The use of 3 points spanning the periapse overlap from either baseline represented an extremely underdetermined system. It is operationally feasible to collect data for a single ΔDOR measurement once every 10 min, including acquiring a nearby quasar. Even with this increased sampling rate a single baseline still performed poorly. However, as we see in Fig. 8(d), when we combine 3 points from each baseline, the results are comparable to our original 2-point strategy when all 9 overlaps from the Goldstone-Canberra baseline were used. One can see that the position uncertainties obtained by the two strategies follow each other reasonably well except near periapse #4. Here our two-baseline periapse strategy performs better because it contains the powerful Goldstone-Madrid periapse data that are naturally missing from the Goldstone-Canberra 2-point strategy. In Fig. 8(e) we see that our ΔDOR periapse strategy determines the 1σ apoapse position to about 285 m, compared to 3800 m for our doppler strategy.

We have decomposed the total 1σ RSS position uncertainty for our ΔDOR periapse strategy into radial, cross-track, and along-track components in Fig. 9. In addition, Fig. 10 shows a similar decomposition of the data noise contribution. Comparison of Figs. 9 and 10 indicates our ΔDOR strategy is dominated by the effects of considered parameters. Also, when one compares the data noise contribution in Fig. 10 to those for doppler in Fig. 5, it is clear that the information content of the ΔDOR measurements allows for two orders of magnitude reduction in data noise.

From the data in Fig. 9 it is evident that the cross-track position component is the best-determined. The rather broad sinusoidal signature peaks near each apoapse and predicts about as well as it is determined. Approximately 90% of the signature amplitude is due to uncertainties in the Earth's geopotential field. We expected the cross-track component to be determined fairly well since our Goldstone-Canberra baseline provided strong out-of-plane information.

The along-track component shown in Fig. 9 exhibits maximum amplitude near periapse, primarily due to uncertainties in the Earth's geopotential field. This trend continues during the predictive phase as well, although atmospheric drag effects grow from a negligible contribution at the beginning of this period to a sizable 40% at the end. By this time atmospheric drag has induced an orbital period uncertainty of about 5 min. We attempted to estimate drag coefficient but found that there was insufficient information content in our ΔDOR measurements to confidently estimate this parameter.

During the definitive time period the radial component exhibits a sinusoidal behavior with maximum and minimum points occurring near alternating periapse epochs. Both extremes are dominated by contributions of the Earth's geopotential field. The predictive position uncertainty peaks near periapse and is also dominated by the effects of the Earth's geopotential field. Like the along-track component, the radial component has a negligible drag contribution at the beginning of the predictive period that grows to about 40% by the end.

The following were accomplished using ΔDOR measurements acquired at periapse by two orthogonal baselines:

(1) The in-plane angular position was defined well by the Goldstone-Madrid baseline;

(2) The orbit orientation was defined well by the Goldstone-Canberra baseline;

(3) Some angular rate information was provided by each baseline because of the large true anomaly changes which occurred during each overlap; and

(4) The sensitivity to gravity harmonics was reduced by the combination of two baselines.

C. Strategies Using DOR

Differenced one-way range (DOR) is acquired in a manner similar to that of ΔDOR, except that quasar acquisition is not necessary. However, the ability to remove errors common to each downlink through double-differencing in also eliminated, and therefore increases the effective measurement noise and bias (see Table 2). With these larger measurement uncertainties we evaluated the performance of the DOR strategy using the same two-baseline periapse data acquisition scenario previously developed for ΔDOR. We observed very little difference in overall performance between DOR and ΔDOR due to the dominant influence of uncertainties in the Earth's geopotential field. These results were obtained using an error magnitude equal to 75% of the lumped parameter difference in two independent geopotential models. Improvement in the geopotential model would directly improve the performance of both the ΔDOR and DOR strategies. We have evaluated the performance of the two strategies, assuming a much smaller error magnitude of 5%, and the results are compared in Fig. 8(f). Both strategies provided substantially improved performance during the definitive phase, but the greatest improvement is realized during the predictive phase. Now the difference in the ΔDOR and DOR performance is due specifically to the differences in the data noise and bias values used for the two strategies.

The capability of the doppler strategy using the JPL geopotential model was compared to our reference case and found to be similar since data noise is the primary source of position uncertainty.

D. Strategies Using Narrowband ΔVLBI

A brief evaluation of the capabilities of narrowband ΔVLBI showed that the performance of this measurement type is very similar to that of doppler. Like the other VLBI strategies we have evaluated, NBΔVLBI performance was dominated by uncertainties in the geopotential model. This conclusion is based on the results of a strategy using the same two-baseline periapse scenario we used for ΔDOR. Although this strategy performs no better than doppler, it is possible to achieve this capability with only 3 measurements from each of two periapse overlaps, compared to a much larger antenna commitment required for the doppler strategy.

VI. Conclusions

The results of our covariance analysis demonstrate that for an IRM-type Earth orbiter, an order-of-magnitude improvement in definitive position accuracies can be achieved using VLBI data in place of doppler with a significant reduction in antenna support requirements. There is a 10:1 reduction in the number of data acquisition passes and a 100:1 reduction in the total number of measurements.

By evaluating the sensitivity of VLBI measurements in terms of orbit geometry we found that data acquired near periapse performed best due to the large true anomaly changes across the overlap. The use of two orthogonal baselines defined both the in-plane angular position and the orbit plane orientation.

We showed that ΔDOR and DOR strategies performed similarly due to the dominant influence of uncertainties in the Earth's geopotential field. Even when the navigation performance was evaluated for an improved geopotential model, it was found that the difference in ΔDOR and DOR capabilities was not significant. As a result it would be feasible to use DOR strategies in place of ΔDOR and avoid the requirement for a nearby quasar. The use of NBΔVLBI does not show the same potential as ΔDOR and DOR, although it can match doppler performance with much less antenna support.

Based on the results of this study the use of VLBI and ΔVLBI measurements for navigating a highly elliptical Earth orbiter like the AMPTE/IRM appears very promising. The AMPTE mission will be launched in August 1984 and at that time it may be possible to conduct in-flight demonstrations and compare the results with those presented here.

Acknowledgement

The authors wish to express appreciation to M. C. Hanna, J. A. Kechichian and C. S. Christensen for their contributions to this work.

References

1. Melbourne, W. G., and Curkendall, D. W., "Radio Metric Direction Finding: A New Approach to Deep Space Navigation," AAS/AIAA Astrodynamics Specialist Conference, Jackson Hole, WY, September 1977 (unnumbered paper).

2. Border, J. S., Donivan, F. F., Finley, S. G., Hildebrand, C. E., Moultrie, T. and Skjerve, L. J., "Determining Spacecraft Angular Position with ΔVLBI: The Voyager Demonstration," AIAA Paper No. 82-1471, AIAA/AAS Astrodynamics Conference, San Diego, CA, August 1982.

3. Curkendall, D. W., "Radio Metric Technology for Deep Space Navigation: A Development Overview," AIAA Paper No. 78-1395, AIAA/AAS Astrodynamics Conference, Palo Alto, CA, August 1978.

4. Yunck, T. P. and Wu, S. C., "Orbit Determination of Geosynchronous Satellites by VLBI and ΔVLBI," AIAA Paper No. 82-1446, AIAA/AAS Astrodynamics Conference, San Diego, CA, August 1982.

5. Frauenholz, R. B., "Tracking and Orbit Determination Strategies for the AMPTE Mission Set," AIAA Paper No. 82-0206, AIAA 20th Aerospace Sciences Meeting, Orlando, FL, January 1982.

Table 1. DSN station viewperiod overlaps (reference epoch: 8/13/84, 07:33:10 GMT)

Overlap number	Goldstone-Canberra Baseline			Goldstone-Madrid Baseline		
	Orbit number	Duration (hh:mm)	True anomaly change, deg	Orbit number	Duration (hh:mm)	True anomaly change, deg
1	1	03:41	4.06	1	03:08	5.21
2	1	*	*	1	01:04	2.25
3	2	03:42	3.89	2	02:46	3.39
4	3	02:04	112.11	2	*	*
5	3	03:40	4.06	3	02:27	2.63
6	4	03:31	11.69	3	*	*
7	4	03:37	4.75	4	02:09	2.27
8	5	03:39	6.24	4,5	04:54	274.86
9	5	03:29	6.55	5	01:46	2.04
10	6	03:41	4.64	6	03:10	8.58
11	6	*	*	6	01:11	1.72
12	7	03:41	4.02	7	02:46	4.26
13	7	*	*	7	*	*

*Not visible

Table 2. Navigation system error model

Error source	One-Sigma uncertainty
Earth geopotential field	75% of SAO-APL 8 x 8 model difference to consider; 100% to estimate
Earth *GM*	$GM \times 10^{-6}$
Lunar *GM*	$GM \times 10^{-6}$
Lunar ephemeris	100 m each axis
Drag coefficient	50% of nominal to consider 100% of nominal to estimate
Solar pressure	10% of nominal reflectivity
Solar flux	30% of nominal
Tropospheric refraction	10% of nominal
Station timing error	1 ms
Station location	
For doppler/range:	
Local X and Y	5 m
Local Z	15 m
For VLBI data types	0.8 m interstation baseline
Two-way doppler noise	2 cm/sec
Range (continuous wave)	
Noise	1000 m (deweighted)
Bias	15 m
ΔDOR	
Noise	0.15 m
Bias	0.20 m
DOR	
Noise	0.3 m
Bias	3.1 m
NBΔVLBI noise	0.1 mm/sec

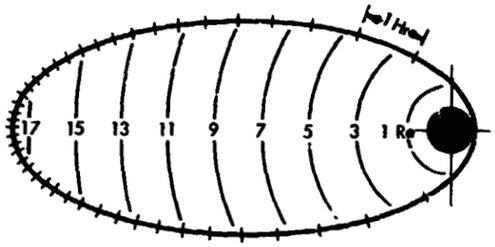

Fig. 1. Time and altitude history of the reference orbit

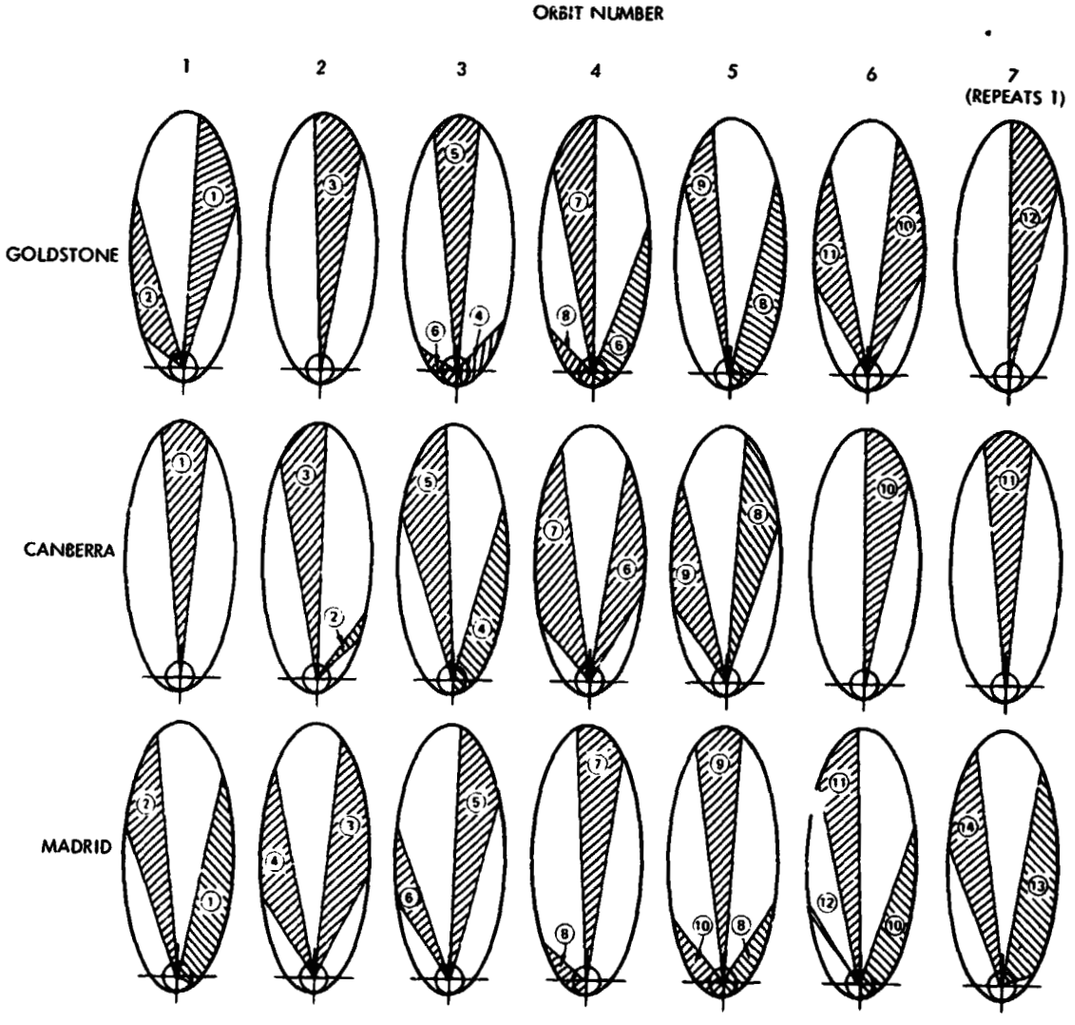

Fig. 2. DSN viewperiods of the reference orbit (minimum elevation is 10 deg)

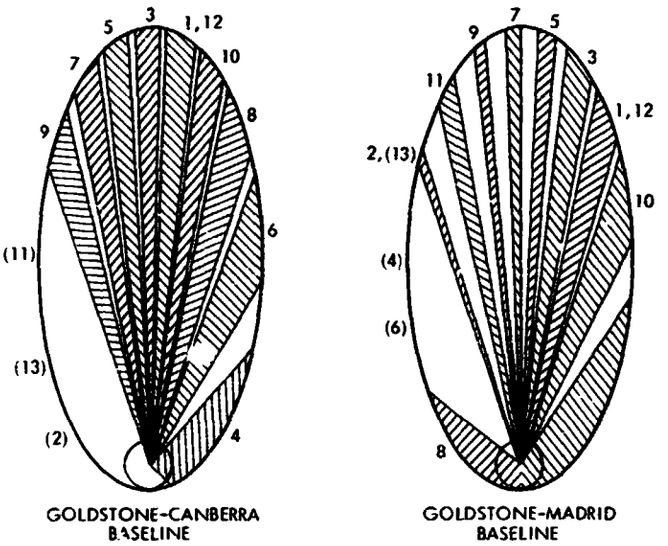

Fig. 3. Composite of DSN viewperiod overlaps for 7-orbit sequence

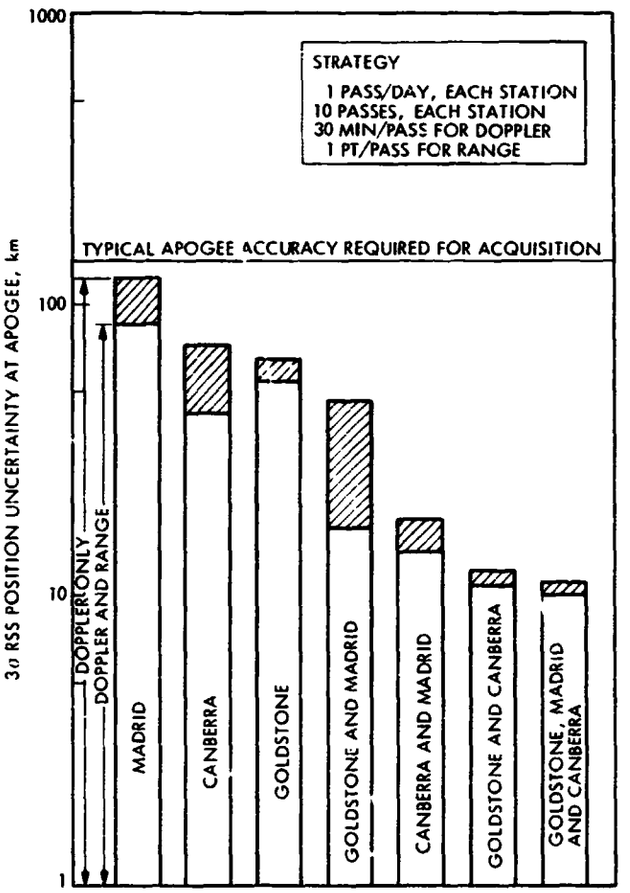

Fig. 4. Accuracy in apoapse position using two-way doppler and range

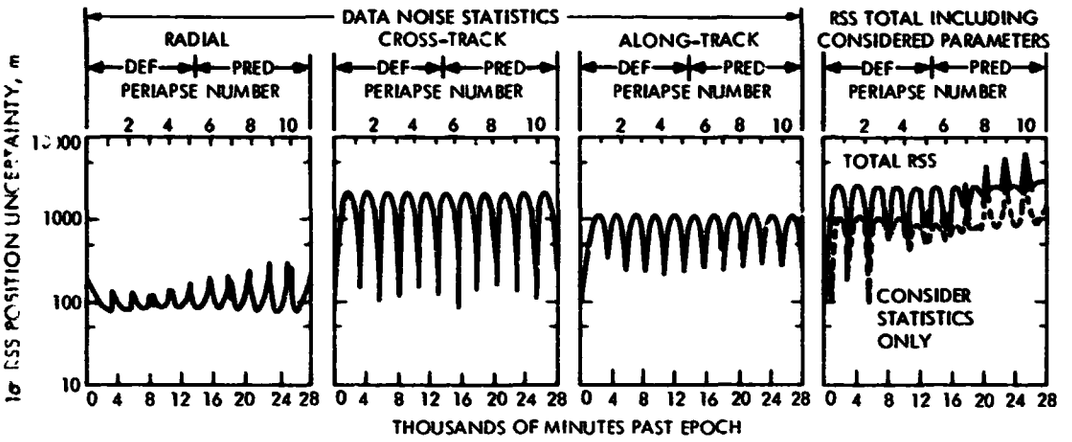

Fig. 5. Position accuracy using doppler from Goldstone and Canberra

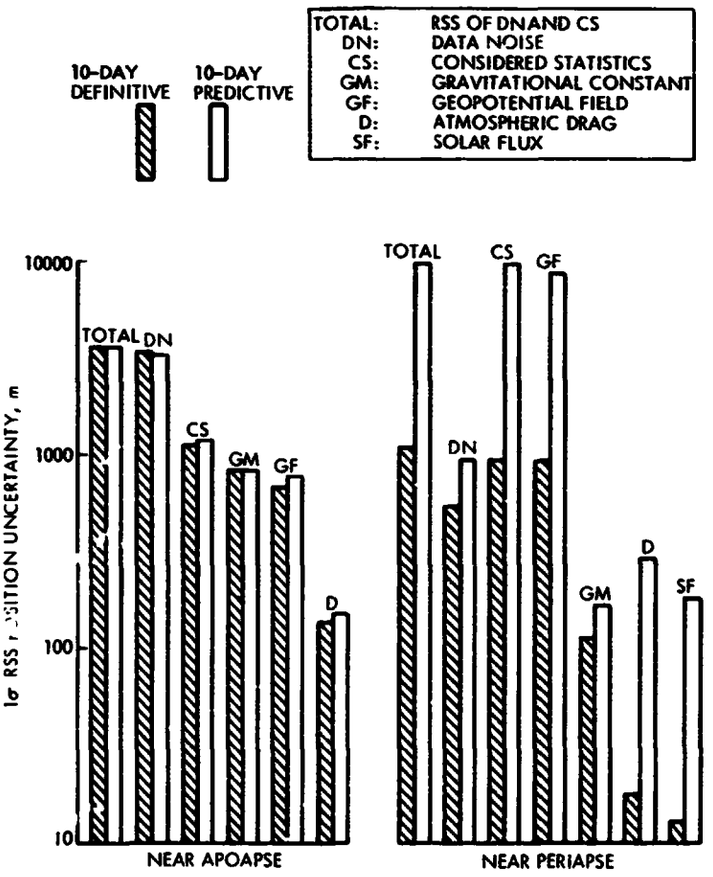

Fig. 6. Comparison of definitive and predictive position accuracies near apoapse and periapse using doppler from Goldstone and Canberra

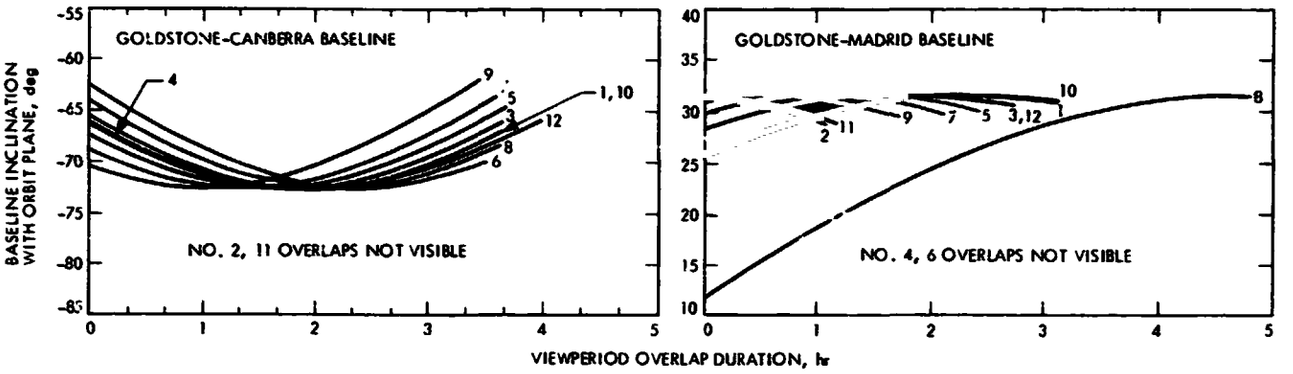

Fig. 7. Baseline inclination with reference orbit plane

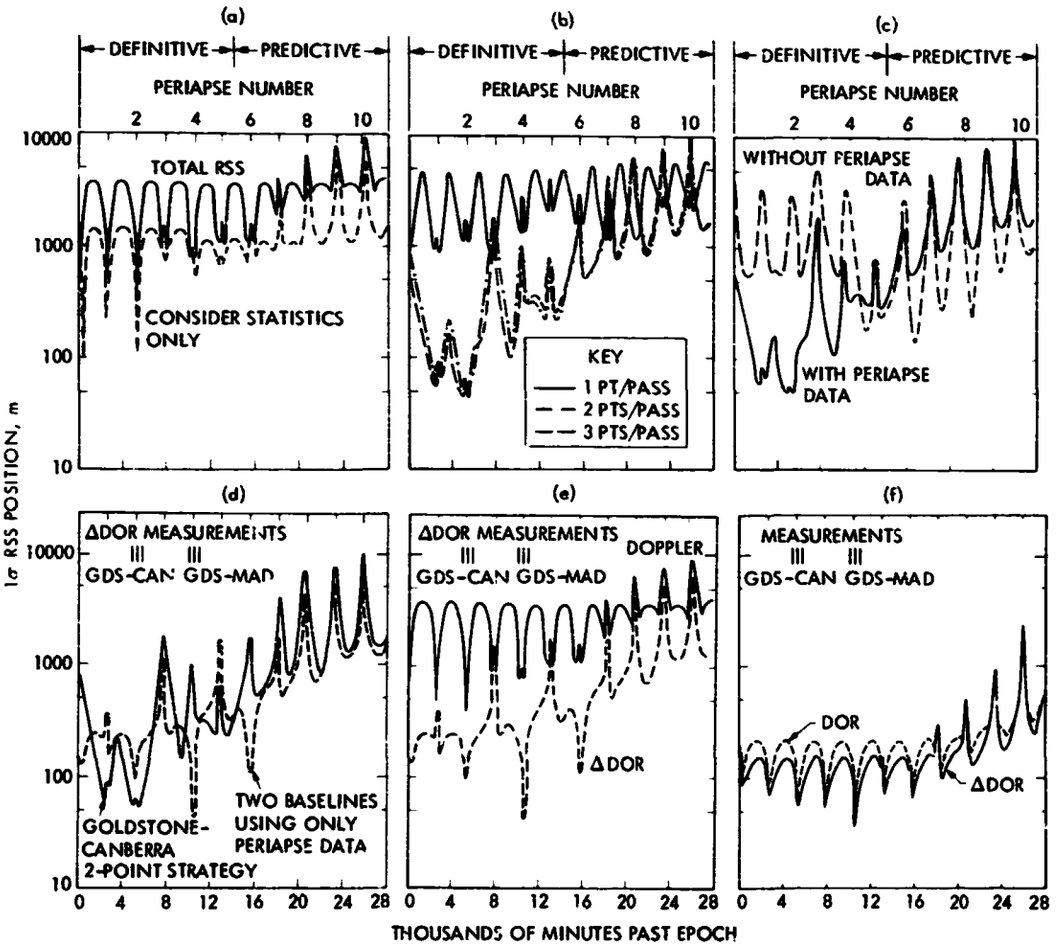

Fig. 8. ΔDOR capability using Goldstone-Canberra baseline: (a) Reference position accuracy using doppler (see Fig. 5); (b) ΔDOR accuracy using 9 overlap passes (see Fig. 3); (c) ΔDOR 2-point strategy with and without periapse data; (d) Two periapse baselines versus 2-point strategy; (e) ΔDOR periapse strategy versus doppler; (f) ΔDOR versus DOR for 5% geopotential model

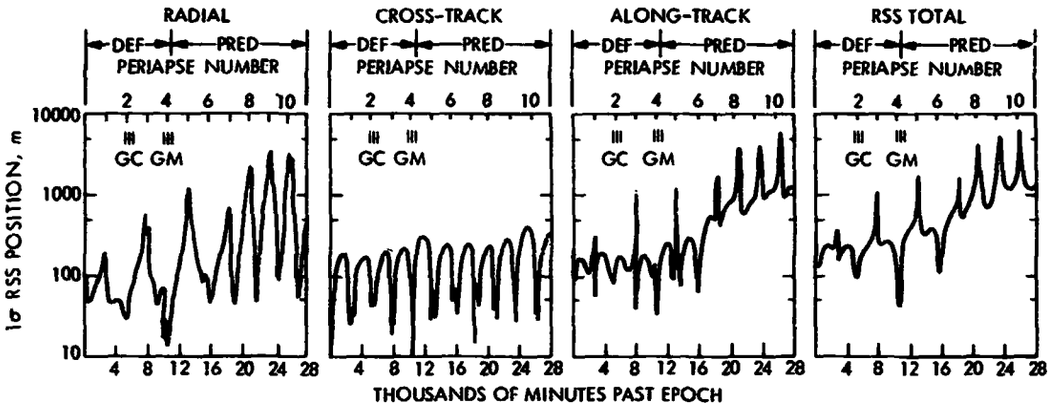

Fig. 9. Radial, cross-track, and along-track components of the ΔDOR periapse strategy

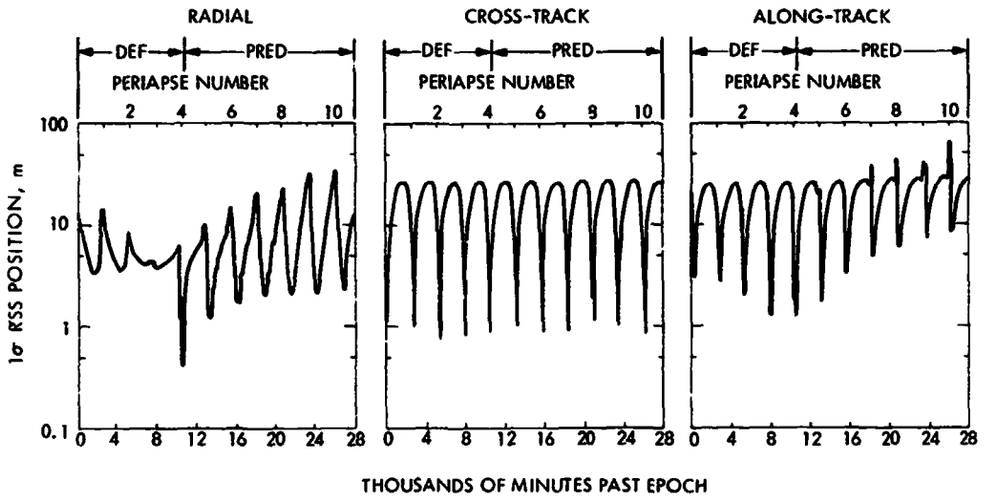

Fig. 10. Components of data noise for the ΔDOR two-baseline periapse strategy